First-principles calculations of small silicon clusters adsorbed on a graphite surface

J. H. Wu,[1] F. Hagelberg,[1] and K. Sattler[2]
[1]*Computational Center for Molecular Structure and Interactions, Department of Physics, Atmospheric Sciences, and General Science, Jackson State University, Jackson, Mississippi 39217, USA*
[2]*Department of Physics, University of Hawaii at Manoa, Honolulu, Hawaii 96822, USA*
(Received 8 February 2005; revised manuscript received 12 May 2005; published 18 August 2005)

The structural and electronic properties of small Si-clusters adsorbed on the graphite (0001) surface are studied by density functional theory (DFT) within periodic boundary conditions. A 5-layer graphite slab is used to represent the graphite substrate. Maximum stability is encountered for particle site adsorption of the Si-clusters on the surface. This finding is attributed to the formation of covalent carbon-silicon bonds. As a consequence of the interaction between the substrate and the adsorbate, a distinct narrowing of the Si cluster energy gap is observed, in accordance with experimental results. Density of states (DOS) distributions are used for detailed band structure analysis of the system combined of Si_n clusters and a graphite substrate. Comparison is made with the analogous situation of the Na_n cluster adsorption on graphite.

DOI: 10.1103/PhysRevB.72.085441 PACS number(s): 61.46.+w, 68.43.Bc, 36.40.Cg

I. INTRODUCTION

The study of adsorbates on semiconductor surfaces and in particular on graphite substrates is an active area of basic research which is highly relevant to present advances of micro- and nanoelectronic technology. In this contribution we focus on Si_n clusters deposited on graphite which is a prototypical layered semimetallic material. Its planar geometry and weak van der Waals interlayer coupling make it possible to split flat, clean surfaces, which are ideal for studying the adsorption of layers and clusters. The interest in these systems is documented by a large number of experimental and theoretical studies on pure graphite as well as cluster adsorption on the graphite surface.[1–16]

Silicon clusters (Si_n) and nanostructures are widely studied due to their fundamental role in cluster physics and chemistry as well as their applications in materials science.[17–21] The optical and electronic properties of these nanosystems are largely governed by the quantum size effect. Thus, the size dependence of the energy gap between the highest occupied molecular orbital (HOMO) and the lowest unoccupied molecular orbital (LUMO) is essential for the understanding of material properties such as intrinsic conductivity and optical transitions. Small Si_n clusters attain maximum energy gap values at certain numbers of constituents, namely $(n=7,10,12)$.[17] The largest energy gap, $E_{gap}=2.18$ eV, is obtained from local density approximation (LDA) calculation for Si_{12}.[17] In a recent experiment, pristine Si clusters were grown on highly oriented pyrolytic graphite (HOPG) upon submonolayer deposition of Si atoms.[22] The scanning tunneling microscopy (STM) technique was used to measure the energy gaps of Si_n clusters. The experimental results reflect a reversal of the commonly assumed trend of an energy gap increase as one goes from the infinite bulk to finite cluster systems.[22] For all experimentally observed Si_n diameters, the measured energy gaps turned out to be sizably smaller than that of bulk silicon (1.1 eV). For smaller cluster diameters, the largest recorded gap amounts to 0.45 eV. Evidently, the interaction between Si_n and the graphite surface will affect the properties of the clusters as well as the properties of the graphite surface.

In the limit of very small clusters, every atom is at the surface. The Si atoms are likely to form bonds with the carbon atoms of the graphite surface. In our previous work, a $Si_5C_{54}H_{18}$ supercluster was used to describe a Si_5 cluster deposited on a graphite layer.[23] Density functional theory computations were performed using the 3-21G* basis set. This work led to a qualitative understanding of the Si_5 energy gap narrowing effect in terms of dimensional reduction of the adsorbed cluster as compared with the gas phase species. This calculation, however, replaced the infinite graphite surface by a fragment of a graphene sheet and thus operated with an inadequate representation of the periodic substrate. In a recent article,[16] periodic boundary conditions were implemented to treat the adsorption of sodium clusters on a graphite substrate. In this work, the geometry of graphite was not optimized due to the failure of the generalized gradient-corrected approximation, which was employed for the exchange-correlation energy functional, to describe the weak van der Waals-type interactions.[14,15] In addition, Si_n clusters are expected to behave quite differently from those composed of alkali metal atoms. Among the basic findings related to the interaction between Na based adsorbates and the graphite substrate is the observation that a single Na atom locates preferentially above a hollow site of the graphite surface. Further, the presence of the substrate modifies the gas phase equilibrium structures of Na_3, Na_4, and Na_5 significantly. A charge transfer of ~ 0.5 electrons, proceeding from the adsorbates to the graphite layer, was found for deposited Na atoms and Na_3 clusters.[16] As far as the geometry of the absorbed clusters as well as their electronic structures are concerned, one expects to find markedly differing results for Si and Na adsorbates, as the bond between Si and C atoms should be covalent, but that between alkali metal and C atoms ionic.

In this contribution, we use a density functional scheme with periodic boundary conditions to model the Si_n clusters adsorbed on the graphite substrate. The substrate consists of five graphene layers, where the first two top layers are fully

optimized, and the three bottom layers are fixed at the optimized bulk structure which represents the semibulk case. The equilibrium structure of the Si_n $(n=1,2,3)$ clusters and the graphite substrate have been obtained by subjecting the slab consisting of the substrate and the adsorbed cluster to total energy optimization. In all investigations, the preceding work on Na cluster adsorption on graphite serves as a standard for comparison.[16] Particular emphasis is put on the structural changes of the Si_n clusters as a result of their interaction with the graphite substrate, as well as the associated changes of the electronic structure. In addition, the full geometric and electronic relaxation of the graphite surface in response to Si cluster deposition is taken into account in this work.

The paper is organized as follows. First the computational method is outlined; subsequently, the calculated results are presented and discussed. Finally, we add some concluding remarks.

II. METHOD

The calculations have been performed using the Vienna *ab initio* Simulation Package (VASP),[24,25] which is based on Density Functional Theory (DFT).[26] More specifically, the finite temperature version of Local Density Functional (LDF) Theory, as developed by Mermin,[27] is utilized in conjunction with the exchange-correlation functional given by Ceperley and Alder and parameterized by Perdew and Zunger.[28] Finite temperature LDF theory introduces a smearing of the one-electron levels and helps to solve convergence problems arising from the use of small sets of **k** points for Brillouin-zone integrations. Unless mentioned explicitly, a Monkhorst Pack[29] **k** point mesh of size $4\times4\times1$ is used for the geometry optimization, and of size $8\times8\times2$ for the density of states (DOS) computations. For the larger supercell, the **k** mesh may be chosen relatively small without substantial sacrifice of accuracy. The period along the z direction of the supercell employed in our calculations is 26.71 Å, while a $p(3\times3)$ pattern is used in the x-y plane.

The **k** point sets indicated above tend to be associated with energy error in the order of meV. The generalized Kohn-Sham equations[26] are solved employing a residual minimization scheme, namely the direct inversion in the iterative subspace (RMM-DIIS) method.[30,31] The optimization of the atomic geometry is performed via conjugate-gradient minimization of the total energy with respect to the atomic coordinates. The interaction of valence electrons and core ions is described by the projector-augmented wave (PAW) method[32] within LDA. Although the generalized gradient approximation (GGA) for the exchange-correlation functional yields more precise results for the system energy than those obtained by LDA, it fails to describe the weak van der Waals-type interactions between the interlayer of the graphite substrate.[14,15] Thus, it does not arrive at a convergent result for the interlayer distance.[15]

The graphite substrate is modeled by slabs with three-dimensional periodic boundary conditions. Two neighboring slabs are separated by a space of more than 10 Å of vacuum. The top two graphite layers are optimized, while the three bottom graphite layers are kept fixed at the optimized bulk values. Thus, the positions of the topmost two layers are allowed to vary within the supercell. Of course, the in-plane positions of the highest two graphite layers are restrained by the size of the supercell due to the periodic boundary conditions. The impact of this limitation is diminished as the supercell size is increased. We therefore considered supercells of different sizes. The deposited Si_n clusters are initially positioned at various well defined sites on the graphite surface, labeled α, β, and hole site in Fig. 1. For the combined system of the adsorbed Si_n clusters and the graphite substrate, we use a $p(3\times3)$ supercell, which consists of 18 atoms per graphene layer. In total, our description of the graphite substrate involves 90 C atoms. To explore the Si coverage effect, we employ supercells of three different sizes and include only one adsorbed Si atom.

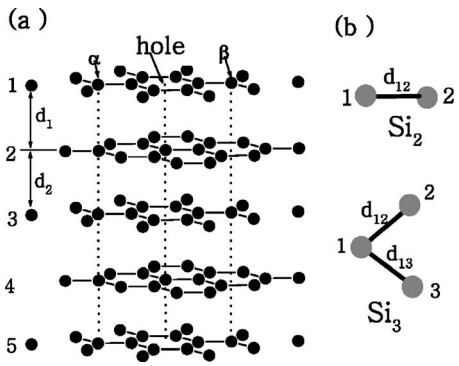

FIG. 1. (a) A 5-layer graphite slab with a $p(3\times3)$ supercell. The α, β, and hole sites are indicated. The distance between the first and the second layer is d_1, and that between second and third layers d_2. (b) The structures of Si_2 and Si_3. The bond length between the ith and the jth atom is denoted by d_{ij}.

In order to obtain accurate adsorption energy results, we use the same parameters for all calculations. For the plane wave functions, an energy cutoff $E_{cut}=400$ eV is used. This choice is justified since it provides correct results for the structures of the graphite bulk, the graphite slab and the Si_3 cluster, as is further outlined in Sec. III. Investigating the adsorption of one Si atom on the graphite surface, we compared different cutoff energies, namely $E_{cut}=400$, 500, and 1000 eV. In each case, the adsorption energy was computed. From this study, we find that the adsorption energy as a function of E_{cut} varies by less than 15 meV for all cases considered. For the partial occupancies of each wave function, the tetrahedron method with Blöchl corrections method[33] is used. The smearing width for the finite temperature LDA is set to $\sigma=0.01$ eV. Reducing the temperature and decreasing σ from 0.01 and 0.0001, we recorded a change of less than 5 meV in the adsorption energy of a single Si atom deposited on the graphite surface for all cases. To examine the partial optimization method used in this work, associated with frozen atomic positions in the three lowest graphene layers, we reinvestigated all cases involving atomic Si deposition on graphite in the $p(3\times3)$ frame as well as Si_3 deposition parallel to the graphite surface without applying any geometric constraints. Both approaches, i.e., the full and the partial optimization, were found to yield the same results

TABLE I. The structural parameters of the bulk and of the five layer graphite slab used in this work.[a]

		Our results	Ref. 15	Experimental[b]
bulk	a (Å)	2.446	2.450	2.460
	c (Å)	6.678	6.500	6.700
	C-C (Å)	1.412	1.415	1.420
slab	a (Å)	2.446		
	d_1 (Å)	3.339		
	d_2 (Å)	3.339		

[a]The symbol a stands for the lattice constant in the graphite plane, c is the lattice constant in the vertical direction of graphite, and C-C is the bond length between two carbon atoms. The distances d_1 and d_2 are defined in Fig. 1.
[b]Reference 35.

within the accuray of the energy convergence criterion of 1.0 meV, thus justifying our approximation of keeping the lowest three slab layers frozen.

III. RESULTS AND DISCUSSION

In this section, we will first present our findings on the pure graphite surface and subsequently turn to three distinct cases of Si_n adsorption on graphite. Thus, we will outline our results for single Si atoms, Si_2 molecules, and Si_3 clusters interacting with the graphite substrate.

Considering the pure graphite surface, we have calculated the optimized bulk lattice constants using the LDA formalism in conjunction with ionic pseudopotentials. The results of this computation, as listed in Table I, are close to those given in Ref. 15. These parameters are used as geometric constraints for the three bottom layers of the five layer graphite slab employed in all computations that form the topic of this study. All remaining distances and angles, i.e., those pertaining to the two top graphite layers are allowed to vary during optimization. The results of this calculation demonstrate that the structure of the two top layers does not deviate from that of the bulk (see Table I). The two top graphite layers are found to remain planar. The same results are obtained as all five graphene layers are included in the optimization. The surface energy amounts to $\sigma \approx 0.42$ eV within the supercell $p(3\times3)$. As 18 atoms are included in each layer, the surface energy per surface atom is about 0.023 eV. This value is substantially smaller than the result of a comparable calculation for diamond[34] where the 2.16 eV/surface atom was obtained. From these findings, the surface layer of graphite does not differ markedly from the inner layers. This conclusion justifies an approximate treatment of the graphite surface as a two-dimensional system (Fig. 2).

In order to assess the influence exerted by the graphite surface on the properties of Si_n $(n=1,2,3)$ clusters, we have calculated geometric and electronic properties of pure Si_n clusters. The results are summarized in Table II. These findings are quite similar to the previous results for pure Si_n clusters as derived within the frame of the LDA.[18–21] It should be noted that, by virtue of the periodic boundary conditions used in our calculation, the Si_n clusters are not isolated, but arranged in a periodic array. This approach may induce artificial effects due to the interaction between neighboring clusters. We examine this possibility by comparing the results emerging from the $p(3\times3)$ supercell and a large cell (LC) of dimension 15.0 Å×15.0 Å×15.0 Å, respectively. In the LC, the distance between neighboring Si_n clusters is larger than 12 Å, and thus the interaction between neighboring clusters should be negligible. The bond length of Si atoms in Si_2 decreases by about 0.1 Å as one goes from the $p(3\times3)$ supercell to the LC, and by 0.03 Å in the Si_3 cluster (see Table II).

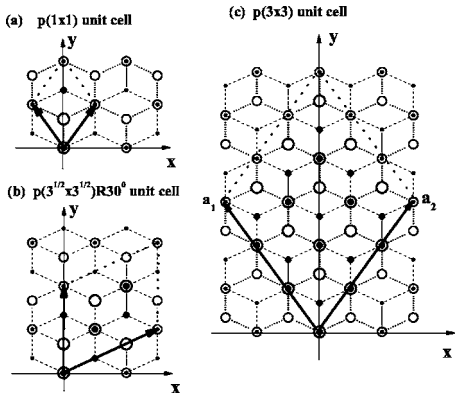

FIG. 2. Top view of the graphite slab. (a) $p(1\times1)$, (b) $p(\sqrt{3}\times\sqrt{3})R30°$, and (c) $p(3\times3)$ unit cells. Hollow circles represent the A-layer of the ABAB graphite structure, solid circles the B-layer. $\mathbf{a_1}$ and $\mathbf{a_2}$ are basis vectors of the $p(3\times3)$ supercell. Heavy symbols denote the atoms in the supercell.

Turning to the energy gap E_{gap}, defined as the difference between the bottom of the conductance band and the top of the valence band, we find an increase by 0.19 eV for the Si_3 cluster. However, the energies of the peaks of conductance and valence bands are almost the same for both choices, $p(3\times3)$ and LC. To rationalize the observed increase of E_{gap} from the former to the latter supercell we invoke the trend of energy band widening as the mutual influence between neighboring clusters strengthens. Since, however, the differ-

TABLE II. The structural and electronic properties of the Si_n $(n=2,3)$ clusters.[a]

			Our results	Ref. 19
Si_2	d_{12} (Å)	$p(3\times3)$	2.29	2.23
		LC	2.19	
	E_{gap} (eV)	$p(3\times3)$	0.0	0.0
		LC	0.0	
Si_3	$d_{12}=d_{13}$ (Å)	$p(3\times3)$	2.20	2.17
		LC	2.17	
	d_{23}	$p(3\times3)$	2.87	2.80
		LC	2.85	
	E_{gap} (eV)	$p(3\times3)$	0.50	0.9
		LC	0.69	

[a]The symbols d_{12}, d_{13}, and d_{23} are defined in Fig. 1, E_{gap} is the energy gap defined in the text.

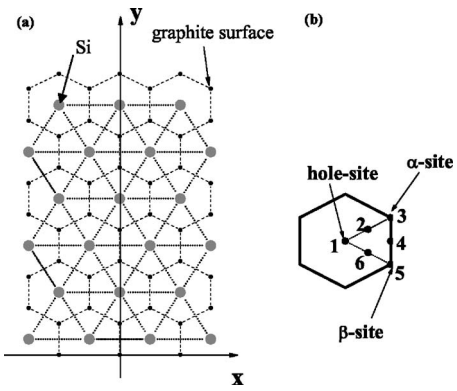

FIG. 3. (a) The top view of Si atoms adsorbed on the graphite surface at hole site within the $p(1\times1)$ unit cell. (b) The different locations of Si adsorbed on the graphite surface.

ence between the results obtained from both supercells is small, it appears justified to investigate the interaction of Si clusters with a graphite substrate adopting the $p(3\times3)$ model.

In order to map the potential energy surface, we have optimized the system with one Si atom adsorbed on the graphite substrate at different initial locations of the Si atom above the surface [Fig. 3(b)]. The coverage effect of the adsorption is considered by using supercells of different sizes, namely $p(1\times1)$, $p(\sqrt{3}\times\sqrt{3})R30°$, and $p(3\times3)$. The distances between two neighboring Si atoms are $d_{\text{Si-Si}}=2.446$ Å, 4.237 Å, and 7.338 Å for the supercells $p(1\times1)$, $p(\sqrt{3}\times\sqrt{3})R30°$, and $p(3\times3)$, respectively. Table III summarizes the results. The positions of the C atoms in the top two graphite layers relax to new equilibrium positions defined by the interaction between the Si atom and the graphite surface. It is found that the surface parallel C atom coordinates stay approximately constant, while the atoms move towards the Si adsorbate in the direction perpendicular to the surface. The vertical positions of the first and second surface layers as indicated in Table III refer to averages over all atoms in the respective layer. The top layer C atoms which are closest to the Si atom position undergo the largest displacement.

Commenting on the effects related to the Si atom coverage of the graphite substrate, we note from the data in Table III that the adsorption energy decreases as the Si atom coverage is enhanced. In addition, the separation of Si atoms from the graphite surface increases with the coverage. In case of the $p(1\times1)$ unit cell, the Si atoms arrange themselves in a distinct two-dimensional pattern with six neighboring atoms surrounding each center, as shown for the example of hole site adsorption in Fig. 3(a). We arrive at an interaction energy of $E_{\text{Si}}=-4.599$ eV/atom for the free Si layer. It is smaller than that of the bulk diamond structure of Si as well as the fcc bulk structure which we determine to be $E_{\text{Si}}=-5.960$ eV/atom and $E_{\text{Si}}=-5.521$ eV/atom, respectively. It surpasses, however, the interaction energies of Si_2 and Si_3 clusters, $E_{\text{Si}}=-2.475$ eV/atom and $E_{\text{Si}}=-3.663$ eV/atom, respectively. The adsorption energy of one Si atom adsorbed on the graphite surface averages to $E_{\text{adsorp}}=0.045$ eV for all different Si locations. The adsorption energy variation between different locations is found to be extremely small, not exceeding 9 meV, corresponding to a rather flat segment of

TABLE III. The structural and electronic properties for Si atom adsorption on the graphite surface.[a]

	Location	d_2	d_1	$d_\perp$	E_{Si}	E_{adsorp}
$p(1\times1)$	1	3.339	3.333	3.290	−4.599	0.045
	2	3.339	3.332	3.292	−4.599	0.043
	3	3.344	3.173	3.554	−4.599	0.050
	4	3.340	3.333	3.288	−4.599	0.041
	5	3.332	3.142	3.416	−4.599	0.043
	6	3.340	3.331	3.294	−4.599	0.043
$p(\sqrt{3}\times\sqrt{3})$	1	3.334	3.305	1.939	−1.548	0.727
	2	3.330	3.308	1.936	−1.548	0.947
	3	3.333	3.306	1.947	−1.548	0.960
	4	3.329	3.296	2.001	−1.548	0.994
	5	3.331	3.304	1.950	−1.548	0.969
	6	3.329	3.307	1.934	−1.548	0.956
$p(3\times3)$	1	3.343	3.327	1.732	−0.066	1.369
	2	3.353	3.302	1.931	−0.066	1.801
	3	3.344	3.309	1.873	−0.066	1.639
	4	3.346	3.311	1.934	−0.066	1.748
	5	3.342	3.323	1.868	−0.066	1.645
	6	3.346	3.312	1.913	−0.066	1.784

[a]The symbols d_1 (Å) and d_2 (Å) are defined in Fig. 1, $d_\perp$ (Å) is the vertical distance between a Si atom and the graphite surface, E_{Si} (eV/atom) the interaction energy between the Si atoms in neighboring supercells, and E_{adsorp} (eV) the adsorption energy.

the potential energy surface. We did not find any deviation of the planar Si atom positions from their initial values. The distance between the Si layer and the graphite surface is $d_\perp = 3.29 - 3.55$ Å. Although the interaction between the Si layer and the graphite surface is weak, the graphite top layer shows some reconstruction. Comparison with the pure graphite surface shows that it moves toward the second layer. With reference to Fig. 3(b), we find the distance between the top and the adjacent layer reduced by 0.18 Å if Si is positioned at sites 3 or 5, and by 0.008 Å if Si occupies the sites 1, 2, 4 or 6.

For the larger supercells $p(\sqrt{3}\times\sqrt{3})R30°$, and $p(3\times3)$, the distance between two neighboring Si atoms increases and their interaction weakens accordingly. For the $p(\sqrt{3}\times\sqrt{3})R30°$ geometry, our result is $E_{\mathrm{Si}} = -1.548$ eV/atom, and $E_{\mathrm{Si}} = -0.066$ eV/atom for the $p(3\times3)$ case. The interaction between the Si atoms and neighboring C atoms on the graphite surface, in turn, gains in strength. The distance between the Si atoms and the graphite surface diminishes as compared to the $p(1\times1)$ coverage, while the planar positions of the Si atoms do not deviate from their initial values for the cases of high symmetry adsorption [Si adsorbed on the positions of 1,3,4 or 5 in Fig. 3(b)]. The Si atom initially located at site 2, with reference to Fig. 3(b), approaches the α site, labeled 3 in Fig. 3(b), while the atoms initially located at position 6 move close to the β site, shown as 5 in Fig. 3(b). There is a slight difference for the adsorption between sites α and β, as well as between sites 2 and 6. Strongest adsorption is observed for a Si atom located at site 4 for the $p(\sqrt{3}\times\sqrt{3})R30°$ supercell and at site 2 for the $p(3\times3)$ cell. The highest adsorption energy differences are found to be 0.267 eV for the $p(\sqrt{3}\times\sqrt{3})R30°$ case and 0.432 eV for $p(3\times3)$ which demonstrates that the related energy potential surface segment is not flat for these two latter configurations, in contrast to our findings for the $p(1\times1)$ supercell, as discussed above. The Si atoms will relax into the positions of maximum adsorption energy on the graphite surface.

This behavior differs from that of sodium atoms adsorbed on the graphite surface.[16] To clarify the origin of the contrasting behavior of the two atomic adsorbates, we analyzed the bonding between the graphite layer and the Si_n clusters, which will be characterized as covalent in the following paragraphs. Commenting further on atomic adsorption, it is interesting that the hole site is not energetically favored for Si, while this arrangement is preferred for the adsorption of sodium atoms.[16] In the latter case, an electron is transferred from Na metal atoms to C atoms, and ionic bonds are formed that stabilize the Na layer on the C substrate. As the graphite hole site is, on comparison with competing sites, deprived of electronic charge density, it is naturally the most favorable location for electron transfer from the alkali metal atom to graphite. However, examination of the respective potential energy surface demonstrates that this preference is not very pronounced. In the case of covalent bonding between adsorbate and substrate, as studied here, positions that allow for high charge density overlap between the partners should be favored. Accordingly, the adsorption energy of Si on graphite is substantially larger than that of Na.

In the following we will comment on our findings related to the adsorption of Si_2 and Si_3 on graphite. In both cases, we distinguish two basic types of adsorption geometries. These consist of a horizontal (vertical) arrangement, involving the plane of Si_3 or the internuclear axis of Si_2 oriented parallel (perpendicular) to the graphite surface. The initial positions of the Si atoms are determined by the high symmetry positions on the graphite surface; i.e, the Si atoms are initially placed near the particle (α and β) or hole sites. A $p(3\times3)$ supercell is used to describe the adsorption of both Si_2 and Si_3 clusters. For both systems the initial structures are defined by the respective cluster equilibrium geometry combined with the condition that the Si atoms are located in close proximity of either particle [α and β in Fig. 1(a)] or hole sites. As discussed above, the potential energy surface for the adsorption of the Si atoms on the graphite substrate is not flat within the $p(3\times3)$ supercell. However, the pattern of potential energy surface minima does not match the structure of the free Si_n, $n=2,3$, clusters. Therefore the final geometry of the composite system results as a compromise between the tendency to preserve the equilibrium structures of Si_n and to occupy the minima of the potential energy surface.

Inspecting first the case of Si_2 adsorption we notice only a minute structural change if parallel adsorption is realized. The distance between two Si atoms, d_{12}, decreases slightly from 2.29 Å in the pure Si_2 cluster to 2.26 Å in the case of two Si atoms initially located on the particle sites (α or β sites). The vertical distance between the Si_2 unit and the graphite surface is found to be about 2.30 Å. The graphite surface atoms closest to the Si atoms move toward the latter. The corresponding adsorption energy is $E_{\mathrm{adsorp}} = 1.250$ eV which is smaller than that resulting for single Si adsorption. The adsorption energy is still quite large as compared to sodium adsorption on the graphite substrate.[16] The bond between the Si centers of Si_2 reduces the interaction between the substrate and the adsorbate.

The internuclear distance of Si_2 changes slightly more when the Si atoms are initially fixed at the hole sites than at the particle sites. The vertical distance, $d_\perp = 2.98$ Å, is increased by 0.70 Å on comparison with the situation of initial Si atom attachment to particle sites. The adsorption energy for the former alternative, $E_{\mathrm{adsorb}} = 0.332$ eV, is sizably smaller than that associated with particle site adsorption. This is consistent with the results reported above for single Si atom adsorption. Figure 4 displays the charge density as a function of the z-axis for the case of both Si atoms initially located at β sites. It is found that the charge density peak of the graphite surface, labeled 1 in Fig. 4, is lower than those assigned to the inner layers. This behavior is ascribed to the loss of electronic charge density from the graphite surface to the interaction region. The charge density distribution of the Si_2 cluster is broadened, indicating the formation of a covalent bond.

Commenting on vertical adsorption, we find the Si-Si distance decreased from its value in the free Si_2 unit, 2.29 Å, to 2.09 Å and 2.10 Å in hole and particle adsorption conditions, respectively. The adsorption energies are $E_{\mathrm{adsorp}} = 0.446$ eV for the particle and 0.054 eV for the hole site. If the vertical alternative is realized, the interaction between the bottom Si atom and the graphite surface determines the adsorption mechanism. In accordance with our previous discussion, the geometry defining impact of the substrate is less

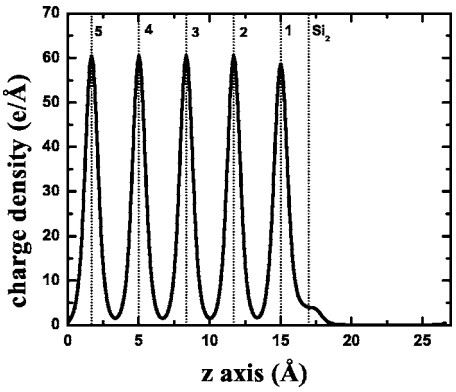

FIG. 4. The charge density distribution along the z-axis in the case of Si_2 initially adsorbed on the β sites of the graphite slab. The dotted lines indicate the positions of the graphite layers and the Si_2 atoms.

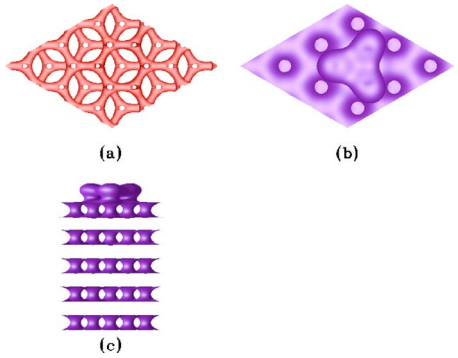

FIG. 5. (Color online) The isosurface of charge densities for parallel adsorption of a Si_3 cluster on the β site of the graphite surface. (a) Topside view with charge density $\rho=15\ e/\text{Å}^3$. (b) Topside view with density $\rho=3\ e/\text{Å}^3$. (c) Frontside view with density $\rho=3\ e/\text{Å}^3$.

pronounced for hole than for particle site adsorption.

The Si_3 cluster adsorption on the graphite substrate is also calculated within the $p(3\times3)$ supercell. The results are summarized in Table IV. In agreement with the trends outlined so far, the condition for maximally stable adsorption is encountered if all Si atoms are initially located near the β sites of the graphite substrate, with the Si_3 plane parallel to the surface. A clear preference of α site over hole site adsorption is found, while the β site turns out to be more stable than the α site by a small margin of 0.044 eV. As mentioned above, the interaction between the Si_3 cluster and the graphite surface is dominated by covalent bond formation. The electronic charge in the neighborhood of the α atoms is slightly depleted along the z-axis, as the result of a transfer to the neighborhood of the β atoms.[15] In view of the slightly higher electronic charge density at the β sites, the covalent bond formed by the Si atoms with the latter is expected to be somewhat stronger than α site bonding. This agrees with our observations. Furthermore, the case of parallel adsorption emerges as more stable than the perpendicular case. The distance between the Si_3 cluster and the graphite surface $d_\perp$ depends sensitively on the adsorption mode. This distance is about 3.3 Å for the hole adsorption which does not induce any substantial change of the Si_3 structure. For particle site adsorption, in contrast, one detects a marked deformation of the Si_3 cluster in response to the strong interaction between the Si atoms and the neighboring C atoms. The internuclear distances are enhanced to match the structure of the potential energy surface minima.

Focusing on vertical adsorption, we only consider the case of two Si atoms bonded to the graphite surface. Within this geometric prototype, we discuss two basic situations: Both Si atoms initially located on hole sites, or one Si atom initially located on the α and the other one on the β site. It is seen from Table IV that the hole site adsorption exceeds the particle site alternative in stability. This can be related to the geometric mismatch between Si_3 and the structure of the substrate in vertical adsorption conditions. Since the distance between neighboring hole sites is 2.446Å, while d_{23} for the Si_3 cluster is 2.87Å, geometric relaxation from the initial hole site geometry causes the Si atoms to adopt a different configuration as they move close to position 4 as indicated in Fig. 3(b). As discussed in the context of single Si atom adsorption, this position is strongly preferred over the hole site. It should be mentioned that the adsorption energy for the Si_2 cluster is smaller than that found for the comparable variant of single Si atom coverage as well as for Si_3 cluster adsorption; the energy difference between these cases, however, is quite small.

For inspection of the covalent bonds between the Si atoms and C atoms on the graphite surface, we plot the charge density isosurfaces for a Si_3 cluster adsorbed on the β sites of graphite in Fig. 5. Only valence electrons are taken into account in our approach. Figure 5(a) displays the in-plane σ bonds connecting adjacent C atoms, constructing a hexagonal structure within the graphene layers. Reducing the isosurface parameter chosen to visualize the σ bonds by a factor of 5, we obtain a representation of the π bonds [see Figs.

TABLE IV. The structural and electronic properties for Si_3 adsorption on the graphite surface.[a]

	Location	d_{12}	d_{13}	d_{23}	$d_\perp$	E_{adsorp}
Parallel	α	2.41	2.41	2.41	2.21	0.350
	β	2.41	2.41	2.42	2.22	0.394
	hole	2.18	2.18	2.80	3.29	0.278
Vertical	α-β	2.17	2.17	2.92	3.08	0.292
	hole	2.17	2.17	2.78	3.04	0.309

[a]For the definitions and units of the symbols d_{12}, d_{13}, d_{23}, $d_\perp$, and E_{adsorp} see the legends of Tables II and III.

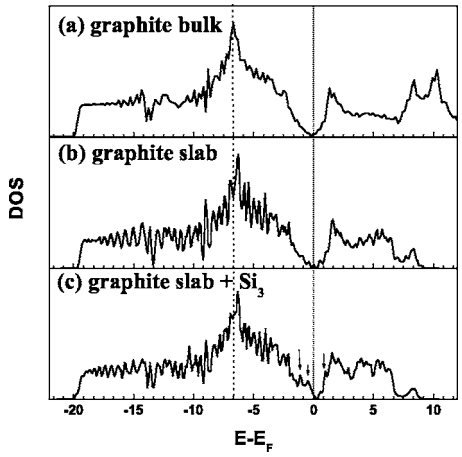

FIG. 6. The DOS of graphite bulk, a 5-layer graphite slab, and 5-layer graphite slab in combination with an adsorbed Si_3 cluster. The Si_3 cluster is arranged parallel to the graphite surface and attached to the β sites.

5(b) and 5(c)] which are oriented perpendicularly to the graphene sheets. The graphite surface is not planar, as it corrugates upon adsorption of Si_3 cluster. The C atoms neighboring the Si atoms are displaced towards the Si atoms, forming covalent π bonds with them, while the second graphene layer is almost unaffected by the adsorbed structure and remains nearly flat.

Now let us turn to the density of states (DOS) distribution. The DOS of bulk graphite, a 5-layer graphite slab, and a Si_3 cluster adsorbed by a 5-layer graphite slab are plotted in Fig. 6. We consider here the case of maximally stable Si_3 adsorption. Obviously the DOS of graphite bulk is quite different from that of the slab as well as the slab with an adsorbed Si_3 unit. The DOS peaks of the slab and the slab in combination with Si_3 exhibits a slight shift of about 0.4 eV to higher energy. This shift is a consequence of the surface energy. As indicated above, the surface energy of the graphite slab within the supercell $p(3\times3)$ is 0.42 eV. Some additional peaks around the Fermi energy are visible for the DOS of the graphite slab-Si_3 composite as compared with the DOS of the pure graphite slab. These peaks stem from the Si_3 cluster. Subtracting the DOS of the pure graphite slab from that of the composite, the DOS of the adsorbed Si_3 cluster alone is obtained. Figure 7 shows the DOS of the Si_3 cluster generated by this technique in conjunction with that of the pure Si_3 cluster. The peaks of the DOS are located at quite similar positions in both cases, excepting the regime of energies $E\geqslant0.8$ eV. However, the deviations between both spectra are pronounced, implying that the interaction between Si_3 and graphite plays a defining role for the electronic properties of the Si_3 cluster. Thus, the full widths of the DOS peaks at half maximum tend to be larger for the difference DOS spectrum than for that of the pure Si_3 cluster. In the difference spectrum the first peak above the Fermi energy is much lower than the corresponding peak in the DOS for pure Si_3. Further, the energy gap between the bottom of conductance and top of valence band for Si_3 obtained from the difference spectrum is seen to be smaller by 0.12 eV than that of the pure Si_3 cluster. Thus, in case of maximally stable

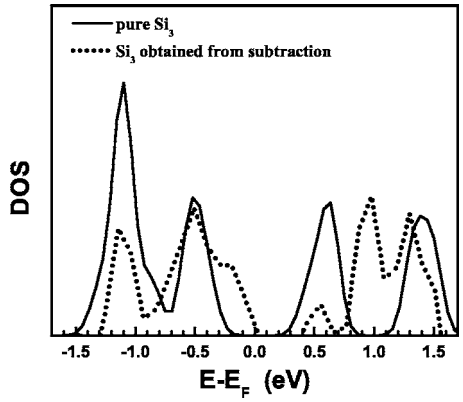

FIG. 7. The DOS of pure Si_3 in comparison with the difference spectrum obtained by subtracting the DOS of the pure graphite slab from the graphite slab with attached Si_3.

Si_3 adsorption on graphite, as identified in this work, the energy gap of Si_3 is about $E_{gap}=0.4$ eV which is in the range of the experimental results.[22]

IV. CONCLUSION

We have analyzed the adsorption of Si atoms and small Si_n clusters with $n=2,3$, on a graphite substrate by use of Density Functional Theory within periodic boundary conditions. The results show that the deposition of Si_n clusters, $n\leqslant3$, on particle sites of graphite gives rise to adsorption structures of higher stability than found for the analogous problem of alkali metal atom clusters on graphite[16] as documented by sizably higher adsorption energies in the former than in the latter case. Covalent bonding is found between the Si_n clusters and the graphite substrate. There is no charge transfer from Si_3 clusters to graphite substrate, in agreement with experimental results.[22] The structural and electronic properties of the deposited Si_3 clusters are strongly affected by their interaction with the graphite substrate. In particular, the energy gap of Si_3 cluster shrinks due to the strong interaction between the Si_3 cluster and the graphite surface, as is demonstrated by comparison of the DOS spectra for the Si_3 unit and the Si_3-graphite composite. The Si_3 energy gap results as 0.4 eV which is in the range of the experimental results.[22] The structure of the Si_3 cluster is strongly deformed to match the graphite surface geometry. The graphite substrate, in turn, reconstructs, albeit slightly, under the influence of the Si_3 adsorbate.

It is envisaged to continue the present work into the size range of Si_n clusters with $n>3$. Thus, a combination of theory and experiment has yielded detailed information about equilibrium structures of Si_n clusters with $n<20$, providing reference geometries for this project.[36,37] The particular challenge of the respective computations consists of the large supercell sizes required to ensure that the interaction between neighboring clusters is sufficiently small. We further plan to investigate silicon-carbon mixed clusters along the lines of the study presented in this contribution. SiC compounds exhibit unusual properties such as extraordinary hardness and variable band gaps;[38] correspondingly, highly

versatile novel nanostructures can be expected to emerge from their combination with graphite surfaces.

ACKNOWLEDGMENTS

This work is supported by the National Science Foundation through Grant Nos. HRD-9805465, NSFESP-0132618, and DMR-0304036, by the National Institute of Health through Grant No. S06-GM008047, and by the Army High Performance Computing Research Center under the auspices of Department of the Army, Army Research Laboratory under Cooperative Agreement No. DAAD 19-01-2-0014.

[1] G. S. Painter and D. E. Ellis, Phys. Rev. B **1**, 4747 (1970).
[2] R. F. Willis, B. Feuerbacher, and B. Fitton, Phys. Rev. B **9**, 2441 (1974).
[3] B. Alzyab, C. H. Perry, C. Zahopoulos, O. A. Pringle, and R. M. Nicklow, Phys. Rev. B **38**, 1544 (1988).
[4] M. Hanfland, H. Beister, and K. Syassen, Phys. Rev. B **39**, 12598 (1989).
[5] D. A. Fischer, R. M. Wentzcovitch, R. G. Carr, A. Continenza, and A. J. Freeman, Phys. Rev. B **44**, 1427 (1991).
[6] P. Zhou and J. E. Fischer, Phys. Rev. B **53**, 12643 (1996).
[7] H. J. F. Jansen and A. J. Freeman, Phys. Rev. B **35**, 8207 (1987).
[8] L. Lang, S. Doyen-Lang, A. Charlier, and M. F. Charlier, Phys. Rev. B **49**, 5672 (1994).
[9] Alex Zunger, Phys. Rev. B **17**, 626 (1978).
[10] N. A. W. Holzwarth, S. G. Louie, and S. Rabii, Phys. Rev. B **26**, 5382 (1982).
[11] J. Furthmuller, J. Hafner, and G. Kresse, Phys. Rev. B **50**, 15606 (1994).
[12] J.-C. Charlier, X. Gonze, and J.-P. Michenaud, Phys. Rev. B **43**, 4579 (1991).
[13] J. C. Boettger, Phys. Rev. B **55**, 11202 (1997).
[14] Y.-H. Kim, I.-H. Lee, S. Nagaraja, J.-P. Leburton, R. Q. Hood, and R. M. Martin, Phys. Rev. B **61**, 5202 (2000).
[15] K. R. Kganyago and P. E. Ngoepe, Phys. Rev. B **68**, 205111 (2003).
[16] K. Rytkönen, J. Akola, and M. Manninen, Phys. Rev. B **69**, 205404 (2004).
[17] Z. Y. Lu, C. Z. Wang, and K. M. Ho, Phys. Rev. B **61**, 2329 (2000).
[18] D. Tománek and M. A. Schlüter, Phys. Rev. Lett. **56**, 1055 (1986).
[19] D. Tománek and M. A. Schlüter, Phys. Rev. B **36**, 1208 (1987).
[20] K. Raghavachari and V. Logovinsky, Phys. Rev. Lett. **55**, 2853 (1985).
[21] G. Pacchioni and J. Koutecký, J. Chem. Phys. **84**, 3301 (1986).
[22] B. Marsen, M. Lonfat, P. Scheier, and K. Sattler, Phys. Rev. B **62**, 6892 (2000).
[23] F. Hagelberg, C. Xiao, B. Marsen, M. Lonfat, P. Scheier, and K. Sattler, Eur. Phys. J. D **16**, 37 (2001).
[24] G. Kresse and J. Hafner, Phys. Rev. B **47**, R558 (1993); **49**, 14251 (1994).
[25] G. Kresse and J. Furthmüller, Comput. Mater. Sci. **6**, 15 (1996).
[26] W. Kohn and L. J. Sham, Phys. Rev. **140**, A1133 (1965).
[27] N. D. Mermin, Phys. Rev. **140**, A1141 (1965).
[28] J. P. Perdew and A. Zunger, Phys. Rev. B **23**, 5048 (1981).
[29] H. J. Monkhorst and J. D. Pack, Phys. Rev. B **13**, 5188 (1976).
[30] D. M. Wood and A. Zunger, J. Phys. A **18**, 1343 (1985).
[31] P. Pulay, Chem. Phys. Lett. **73**, 393 (1980).
[32] P. E. Blöchl, Phys. Rev. B **50**, 17953 (1994).
[33] P. E. Blöchl, O. Jepsen, and O. K. Andersen, Phys. Rev. B **49**, 16223 (1994).
[34] Y. Qi and L. G. Hector, Jr., Phys. Rev. B **69**, 235401 (2004).
[35] R. Nicklow, N. Wakabayashi, and H. G. Smith, Phys. Rev. B **5**, 4951 (1972).
[36] A. Shvartsburg, B. Liu, M. F. Jarrold, and K. M. Ho, J. Chem. Phys. **112**, 4517 (2000).
[37] C. Xiao, F. Hagelberg, and W. A. Lester, Phys. Rev. B **66**, 075425 (2002).
[38] M. Pellarin, C. Ray, P. Mélinon, J. Lermé, J. L. Vialle, P. Kéghélian, A. Perez, and M. Broyer, Chem. Phys. Lett. **277**, 96 (1997).